



**HAL**  
open science

## Nature-inspired synthetic oligourea foldamer channels allow water transport with high salt rejection

Chiranjit Dutta, Pannaga Krishnamurthy, Dandan Su, Sung Hyun Yoo, Gavin W Collie, Morgane Pasco, Jan K Marzinek, Peter J Bond, Chandra Verma, Axelle Grélard, et al.

► **To cite this version:**

Chiranjit Dutta, Pannaga Krishnamurthy, Dandan Su, Sung Hyun Yoo, Gavin W Collie, et al.. Nature-inspired synthetic oligourea foldamer channels allow water transport with high salt rejection. Chem, 2023, 9 (8), pp.2237-2254. 10.1016/j.chempr.2023.04.007 . hal-04257802

**HAL Id: hal-04257802**

**<https://hal.science/hal-04257802v1>**

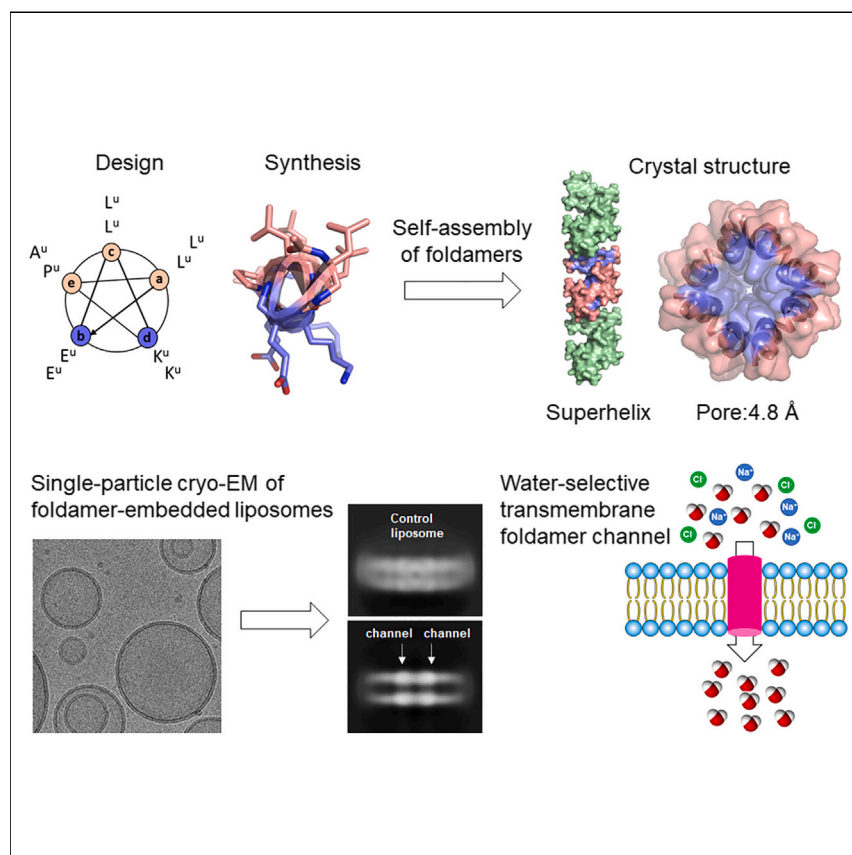
Submitted on 27 Oct 2023

**HAL** is a multi-disciplinary open access archive for the deposit and dissemination of scientific research documents, whether they are published or not. The documents may come from teaching and research institutions in France or abroad, or from public or private research centers.

L'archive ouverte pluridisciplinaire **HAL**, est destinée au dépôt et à la diffusion de documents scientifiques de niveau recherche, publiés ou non, émanant des établissements d'enseignement et de recherche français ou étrangers, des laboratoires publics ou privés.

## Article

## Nature-inspired synthetic oligourea foldamer channels allow water transport with high salt rejection



Short helical amphipathic oligourea foldamers were designed with distinct hydrophobic and hydrophilic faces. Two of the foldamers (H2OC1 and H2OC2) obtained by solid phase synthesis self-assembled into channel-type nanostructures that show efficient water permeability across lipid membranes while rejecting ions. A self-assembled quaternary structure with two superhelical scaffolds results in the formation of 4.8 and 6.4 Å inner pores that were observed in the crystal packing of H2OC1. Both pores have hydrophilic interior and hydrophobic exterior surfaces. Our findings demonstrate the channel-forming ability of oligourea foldamers in lipid bilayers, and such novel artificial water channels could be beneficial for water purification applications.

Chiranjit Dutta, Pannaga Krishnamurthy, Dandan Su, ..., Gilles Guichard, R. Manjunatha Kini, Prakash P. Kumar

mihail-dumitru.barboiu@umontpellier.fr (M.B.)  
g.guichard@iecb.u-bordeaux.fr (G.G.)  
dbskini@nus.edu.sg (R.M.K.)  
prakash.kumar@nus.edu.sg (P.P.K.)

## Highlights

Synthetic, self-assembling, helical oligourea foldamers form artificial water channels

ssNMR, MD simulation, and cryo-EM data show proper insertion of foldamers into liposomes

Water-selective channels are formed by oligomerization of the amphipathic foldamers

4.8 Å hydrophilic pore is present in X-ray crystal structure of foldamer H2OC1



Article

# Nature-inspired synthetic oligourea foldamer channels allow water transport with high salt rejection

Chiranjit Dutta,<sup>1,2</sup> Pannaga Krishnamurthy,<sup>1,2</sup> Dandan Su,<sup>3</sup> Sung Hyun Yoo,<sup>4</sup> Gavin W. Collie,<sup>5</sup> Morgane Pasco,<sup>4</sup> Jan K. Marzinek,<sup>6</sup> Peter J. Bond,<sup>1,6</sup> Chandra Verma,<sup>1,6,7</sup> Axelle Grélard,<sup>4</sup> Antoine Loquet,<sup>4</sup> Jianwei Li,<sup>1</sup> Min Luo,<sup>1</sup> Mihail Barboiu,<sup>3,\*</sup> Gilles Guichard,<sup>4,\*</sup> R. Manjunatha Kini,<sup>1,8,\*</sup> and Prakash P. Kumar<sup>1,2,9,\*</sup>

## SUMMARY

**Biomimetic membranes incorporating artificial water channels (AWCs) are being developed for industrial water purification. Designing AWCs to achieve high water permeation with salt rejection is a challenge. We designed and synthesized oligourea foldamers, which form predictable helical structures that can be used to create biomimetic porin-like architectures. Two of these foldamers (H2OC1 and H2OC2) allow superior water permeability and almost total salt rejection across lipid membranes. Solid-state NMR, cryo-EM, and molecular dynamics analyses suggest proper insertion of foldamers into lipid vesicles. The H2OC1 crystal structure shows hydrophilic pores of diameters 4.8 and 6.4 Å. The oligourea helices pack together by hydrophobic and salt bridge interactions to build two channel-like assemblies. Besides their proteolytic stability and microbial resistance, the sequence of foldamers can be tailored to regulate selectivity. The ease of designing, synthesizing, and purifying oligourea foldamers is an added advantage. Our findings can help to develop novel AWCs for water purification applications.**

## INTRODUCTION

Freshwater scarcity currently affects over 4 billion people worldwide and is a growing challenge faced by humanity. High population, industrialization, deforestation, and climate change lead to depletion and contamination of natural water resources, all of which increase the demand for fresh water.<sup>1</sup> Currently, reverse osmosis (RO) membrane and membrane distillation technologies are used to produce ~100 million tons of desalinated water per day from seawater.<sup>1</sup> However, the high energy consumption and overall cost of the existing technologies necessitate the search for better alternatives. In this regard, the aquaporins (AQPs) have been proposed as active components for the fabrication of desalination RO bio-assisted membranes.<sup>2</sup> AQPs are transmembrane proteins that allow high water permeability ( $\sim 10^9$  H<sub>2</sub>O s<sup>-1</sup>) across lipid membranes with the complete rejection of ions and protons.<sup>3</sup> The key structural feature of the AQP hydrophobic interior is a narrow 3 Å diameter pore, composed of a key asparagine-proline-alanine (NPA) motif, enabling the transport of water molecules in a single file.<sup>3</sup> Unfortunately, the development of AQP-based membranes is limited by the long-term protein stability issues under harsh pressure and salinity RO conditions.<sup>1,2</sup>

## THE BIGGER PICTURE

Water scarcity is a global problem. Although reverse osmosis is an effective method for water purification, it is costly and energy intensive. To address this issue, previously, biomimetic membranes have been developed that are embedded with aquaporins (AQPs) or artificial water channels (AWCs). We designed and synthesized helical amphipathic oligourea foldamers as a new class of AWCs that can be a promising alternative to AQPs. Our foldamer monomers do not have a tubular structure, but they self-assemble, generating void space that acts as transmembrane channels, which exhibit selective water permeability. The crystal packing of one of these foldamers shows a porin-like superstructure with a hydrophilic pore of 4.8 Å diameter. The known resistance of oligoureas to proteolytic degradation suggests that they offer long-term stability. Sequence-based tunability of their properties along with their large-scale synthesis can make them a new class of AWCs for water purification.

Artificial water channels (AWCs) constructed from simple molecular components mimic the structures and functions of natural active protein channels. They address the drawbacks of AQPs and could be used to develop robust biomimetic membranes for the future.<sup>2,4</sup> Carbon nanotubes (CNTs) are among the most promising artificial nanostructures for the development of AWC.<sup>5</sup> Both wide- and narrow-diameter CNTs show high water permeability ( $10^9$  and  $10^{11}$  H<sub>2</sub>O molecules/channel s<sup>-1</sup>) and they block anion transport but not cations.<sup>5</sup> The single file water permeability of narrow-diameter CNTs exceeds AQP1 performance by a factor of 6. Indeed pore-lining residues in AQP1 can form H-bonds with incoming water molecules, thus transport rates are limited by kinetics of H-bond breakage and reformation, molecular re-orientation.<sup>5</sup> By contrast, pore walls of CNTs cannot form H-bonds and allow unimpeded water transport.<sup>5</sup> Thus, the narrow diameter of CNTs promises selectivity as their hydrophobic interior permits water transport with low resistance.<sup>6</sup>

Another class of AWCs described is the imidazole-derived I-quartet channels,<sup>7</sup> which form tubular superstructures. These channels build a 2.6–2.8 Å pore similar to AQPs and completely exclude ions except protons.<sup>7,8</sup> The reported water permeability through the I-quartet is  $10^6$ – $10^7$  H<sub>2</sub>O s<sup>-1</sup> per channel in lipid bilayers<sup>9</sup> is promising and has been translated to planar polyamide membranes for desalination with high per area permeability of 2.5–3 LMH/bar while maintaining a high NaCl rejection of 99.8%.<sup>10</sup> Fluorous oligoamide nanorings of polytetrafluoroethylene self-assemble to create nanochannels through stacking.<sup>11</sup> Due to the water repellent property of carbon-fluorine bonds, the interior of these channels is hydrophobic and allows a high rate of water flow and negligible Cl<sup>-</sup> permeability.

Hydrazide-appended pillar[5]arene and PAH have also been employed to develop AWCs due to their unique tubular conformations.<sup>12</sup> Similarly, peptide-appended pillar[5]arenes (PAP[5]s) showed higher permeability ( $10^7$  H<sub>2</sub>O s<sup>-1</sup>).<sup>13</sup> However, the PAH and PAP[5] channels exhibit high ion permeability due to a larger pore diameter of 5 Å, making them un-useful for the fabrication of desalination membranes.<sup>13</sup> Smaller peptide-appended hybrid[4]arene (PAH[4]) have been used to reduce the pore diameter and achieve salt rejection. They showed increased water permeability of  $>10^9$  H<sub>2</sub>O s<sup>-1</sup> similar to AQP and exhibited undetectable ion permeability.<sup>14</sup> Overall, the PAH[4] translocate water outside the channels and their water/salt permselectivity exceeds the requirement for desalination membranes for which the scale-up methods remains to be solved.<sup>14</sup>

Foldamers are synthetic polymers that tend to generate higher-order folded structures and have been employed for developing AWCs. Aromatic helical aquafoldamers, such as pyridine/oxadiazoles,<sup>15–17</sup> polypyridines,<sup>18,19</sup> polyhydrazides,<sup>20</sup> and fluorofoldamer<sup>21</sup> show selective water and ion transport through their interior helical pore up to  $2.7 \times 10^{10}$  H<sub>2</sub>O channel s<sup>-1</sup> with salt rejection, exceeding to that of AQP1.<sup>20</sup>

However, to the best of our knowledge, there has been no attempt to create artificial water channels from sequence-defined proteinomimetic foldamers that are used as scaffolds that self-assemble into precise quaternary nanostructures with intrinsic porosity (i.e., self-assembled foldamer-based porin-like channels).<sup>17–21</sup> N,N'-linked oligoureas are a class of synthetic peptidomimetic foldamers that have been demonstrated to form well-defined helical structures in both organic and aqueous environment akin to regular peptide helices.<sup>22</sup> Amphiphathic sequences with a patch of hydrophobic side chains at the surface of the helix have been shown to self-assemble into various quaternary structures including nanotubular structures.<sup>23–25</sup> These

<sup>1</sup>Department of Biological Sciences, National University of Singapore, Singapore, Singapore

<sup>2</sup>NUS Environmental Research Institute (NERI), National University of Singapore, Singapore, Singapore

<sup>3</sup>Institut Européen des Membranes Adaptive Supramolecular Nanosystems Group, University of Montpellier ENSCM, CNRS, Place Eugène Bataillon, CC 047, 34095 Montpellier, France

<sup>4</sup>University of Bordeaux, CNRS, Bordeaux INP, CBMN, UMR 5248, Institut Européen de Chimie et Biologie, 2 rue Robert Escarpit, 33600 Pessac, France

<sup>5</sup>Discovery Sciences, R&D, AstraZeneca, Cambridge, UK

<sup>6</sup>Bioinformatics Institute (A\*STAR), 30 Biopolis Street, #07-01 Matrix, Singapore 138671, Singapore

<sup>7</sup>School of Biological Sciences, Nanyang Technological University, 60 Nanyang Drive, Singapore 637551, Singapore

<sup>8</sup>Department of Pharmacology, Yong Loo Lin School of Medicine, National University of Singapore, Singapore, Singapore

<sup>9</sup>Lead contact

\*Correspondence: [mihail-dumitru.barboiu@umontpellier.fr](mailto:mihail-dumitru.barboiu@umontpellier.fr) (M.B.), [g.guichard@iecb.u-bordeaux.fr](mailto:g.guichard@iecb.u-bordeaux.fr) (G.G.), [dbskini@nus.edu.sg](mailto:dbskini@nus.edu.sg) (R.M.K.), [prakash.kumar@nus.edu.sg](mailto:prakash.kumar@nus.edu.sg) (P.P.K.)

<https://doi.org/10.1016/j.chempr.2023.04.007>

oligourea sequences were synthesized using solid phase techniques akin to peptide synthesis, from enantiopure activated monomers prepared from amino acid derivatives (building blocks [BBs]).<sup>22,26</sup> The BBs were protected on one side as azides and activated at the other extremity as succinimidyl carbamates (e.g., N<sub>3</sub>-Leu<sup>U</sup>-OSu). In contrast to natural peptides, these foldamers are substantially more resistant to proteolytic degradation due to their oligourea (i.e., non amide) backbone.<sup>27</sup> These different properties make them potential candidates for synthesizing AWCs.

Here, we report the successful design and synthesis of amphiphilic oligourea foldamers, which are able to form transmembrane channels exhibiting high water permeability rejecting all ions. We show that these non-natural oligomers form tunable helical scaffolds self-assembled in Porin-like nanostructures. The state of oligomerization was investigated by mass spectrometry (MS) and transmission electron microscopy (TEM). The molecular insertion into lipid vesicles was investigated by solid-state NMR spectroscopy. We further characterized their water and ion permeability properties in lipid vesicles. Also, we present their three-dimensional structures elucidated by X-ray crystallography. The high water permeability coupled with resistance to proteolytic degradation makes these novel synthetic foldamers possible candidates for industrial water purification applications.

## RESULTS AND DISCUSSION

### Design and synthesis of H2 derivatives

To design transmembrane water channels, we designed H2OC1–H2OC4 scaffolds starting from known self-assembling properties of a previously reported amphipathic helical oligourea foldamer named H2.<sup>23,24</sup> The 10-mer H2 showed extended superhelical structure with two right-handed intertwined superhelices that form a channel in aqueous conditions with hydrophilic interior and a pore diameter of ca. 17 Å due to its global amphipathicity.<sup>23</sup> The oligourea sequence, composed of two pentad repeats, has been designed to form an amphipathic helix with an extended hydrophobic face using the following principles. At positions “a” and “c”: four leucine-type urea residues (Leu<sup>U</sup>) (two in each pentad repeat). At position “e”: proline-type (Pro<sup>U</sup>) residue in the first pentad and alanine-type (Ala<sup>U</sup>) in the second pentad (Figure 1A).

These hydrophobic residues at the exterior surface assist in forming a dense and precise packing during the self-assembly of H2. Additionally, the side chains of four charged residues (two glutamate-type side chains [Glu<sup>U</sup>] at position “b” and two lysine-type side chains [Lys<sup>U</sup>] at position “d”) point into the lumen and form a highly charged interior of the channel. The electrostatic interactions and salt bridges play a major role in the formation of intricate H-bonding networks among proximal and distal oligourea residues and contribute to stabilizing the overall packing.

We designed and synthesized a series of close H2 analogs and carried out their structural and functional analyses (Figures 1 and S1–S5; Table S1). In the first analog, H2OC1, the N-terminal isopropyl group of H2 was replaced by an acetyl group, and the C-terminal methyl urea was replaced by a simple urea termination to reduce the hydrophobicity (Figures 1A and 1B). To understand the local constraining effect of Pro<sup>U</sup>, we prepared a second analog H2OC2 in which Pro<sup>U</sup> is replaced with Ala<sup>U</sup> at position e (Figures 1A and 1B). We have shown that Pro<sup>U</sup> does not interfere significantly with the helicity of oligoureas<sup>23</sup> unlike Pro in peptide chains.<sup>28</sup> In H2OC3, we replaced two Glu<sup>U</sup> with the less hydrophilic Asn<sup>U</sup> at the b sites of pentads (Figures 1A and 1B). Such substitutions were intended to reduce the interaction with water in the

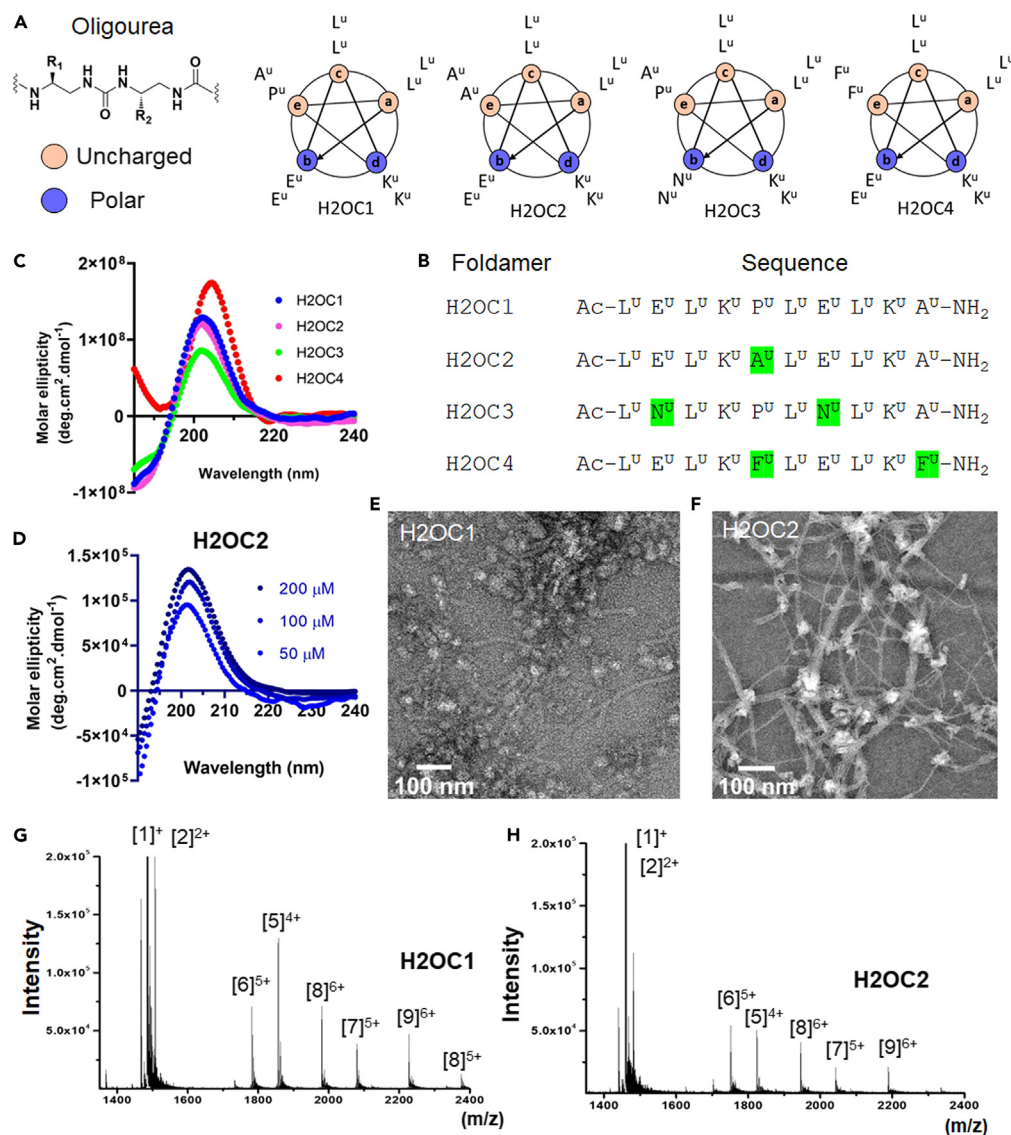


**Figure 1. Molecular design and biophysical characterization of oligourea foldamers**

(A) Helical-wheel representations of designed H2 variants showing the side-chain distribution of oligourea residues in pentad. Polar and charged residues and uncharged residues are depicted as salmon red and cyan blue, respectively.

(B) Sequences of synthesized amphipathic oligourea foldamers H2OC1, H2OC2, H2OC3, and H2OC4. Highlighted residues represent the point mutation to H2OC1.

(C) Circular dichroism (CD) spectra of oligourea foldamers show a peak at ~202 nm indicating their helical conformation.

(D) CD spectra of H2OC2 in water exhibit a concentration-dependent increase of molar ellipticity at ~202 nm.

(E and F) Negative-stained transmission electron micrographs of (E) H2OC1 and (F) H2OC2 revealed self-assembled morphologies at 200 μM in 10 mM HEPES buffer, pH 7.0. They showed fiber-like networks packed in large, knotted bundles (H2OC2, diameter ranging from 12.4 to 40.0 nm) and distinct fibers (H2OC1, diameter 5.5 ± 0.6 nm).

(G and H) Electrospray ionization (ESI) mass spectrometry profiles of (G) H2OC1 and (H) H2OC2. The ESI spectra reveal the distribution of heterogeneous multimeric species of oligoureas. The isotopic peak at *m/z* value of 1,856.76 of H2OC1 indicates pentameric species ([5]<sup>4+</sup>). Other isotopic peaks of multimers are also identified.

polar channel and facilitate faster water flow.<sup>3,29</sup> To enhance the penetration into lipid bilayers, we designed the analog H2OC4 by replacing Ala<sup>U</sup> and Pro<sup>U</sup> residues with Phe<sup>U</sup> at position e in both pentads of H2OC1 (Figures 1A and 1B). Such aromatic Phe-type residues might favorably interact with fatty acyl chains and lipid head

groups.<sup>30</sup> All oligourea foldamers were synthesized on a solid support using microwave assistance (Scheme S1; Table S1; Figures S2–S5) and purified according to previously established procedures.<sup>23,31</sup>

### Biophysical characterization of foldamers

The secondary structure and self-assembly of the foldamers were first investigated by circular dichroism (CD).<sup>32–34</sup> All spectra showed a maximum at ~202 nm (Figures 1C, 1D, and S6), indicating helical conformation of H2OC1 to H2OC4 analogs at 100  $\mu$ M in water.<sup>23,31</sup> They exhibit helicity even at lower concentrations. Concentration-dependent CD experiments of foldamers showed increased molar ellipticity with increasing foldamer concentration, indicating self-assembly in water (Figures 1D and S6).<sup>23,31</sup>

Negative-staining TEM studies of H2OC1 and H2OC2 showed the formation of extensive fiber networks in aqueous conditions (Figures 1E and 1F). H2OC2 showed large fiber bundles with knots (with diameters ranging from ~12 to ~40 nm) consisting of protofilaments with a diameter of  $3.7 \pm 0.8$  nm, whereas H2OC1 showed untangled fibers with a diameter of  $5.5 \pm 0.6$  nm (Figures 1E and 1F). The TEM observations support their fiber-like self-assembly.<sup>23,24</sup> By contrast, H2OC3 showed vesicle-like morphology with about 24–33 nm diameter (Figure S7A). H2OC4 formed longer filaments with about 132–156 nm width (Figure S7C). The stoichiometry of oligourea foldamer self-assemblies was next investigated by MS. Electrospray ionization (ESI)-MS analyses revealed the presence of discrete multimeric species<sup>23,31</sup> ranging from pentamer to nonamer of H2OC1 and H2OC2 in aqueous conditions (Figures 1G and 1H). By contrast, H2OC3 showed a predominant pentameric species (Figure S7B). The TEM and ESI-MS results are thus consistent with H2OC1, H2OC2, and H2OC4 forming helical tubes as previously reported for H2.<sup>23</sup>

### Molecular insertion of foldamer channels into lipid vesicles

To investigate whether H2OC1 and H2OC2 foldamers have the molecular properties to be stably inserted into lipid membranes, we employed solid-state NMR spectroscopy to measure biophysical parameters in a lipid environment. Lipid vesicles composed of a mixture of phosphatidylcholine (PC) and phosphatidylserine (PS) (molar ratio of 4/1) were reconstituted in the presence of H2OC1 and H2OC2 at a molecule-to-lipid ratio of 1/20. To monitor the impact of foldamer insertion into the lipid vesicles, we first used <sup>31</sup>P solid-state NMR to probe the lipid phase and membrane curvature effect. PC/PS vesicles exhibited a <sup>31</sup>P spectral pattern characteristic of a lamellar lipid phase. <sup>31</sup>P experiments carried out for vesicles containing H2OC1 and H2OC2 showed a comparable asymmetric spectral profile and a similar chemical shift anisotropy (Figure 2A), indicating that the lipid phase and the membrane curvature of the vesicles were not significantly impacted by the molecular insertion of the foldamers. To monitor the insertion of foldamers into the hydrophobic part of the lipid bilayer, we used <sup>2</sup>H solid-state NMR on PC/PS vesicles for which the PC acyl chains were deuterated. We detected comparable <sup>2</sup>H quadrupolar couplings for control vesicles and vesicles incorporating H2OC1 and H2OC2 (Figure 2B).

Since <sup>2</sup>H quadrupolar couplings are related to the molecular orientation and the dynamics of the C–<sup>2</sup>H bonds, this suggests that the foldamer insertion has a negligible effect on the internal lipid dynamic at the level of the acyl chain. Lipid thermotropism was evaluated by monitoring the <sup>2</sup>H first spectral moment as a function of the sample temperature (Figure 2C). We observed that the melting temperature ( $T_m = 285$  K) of

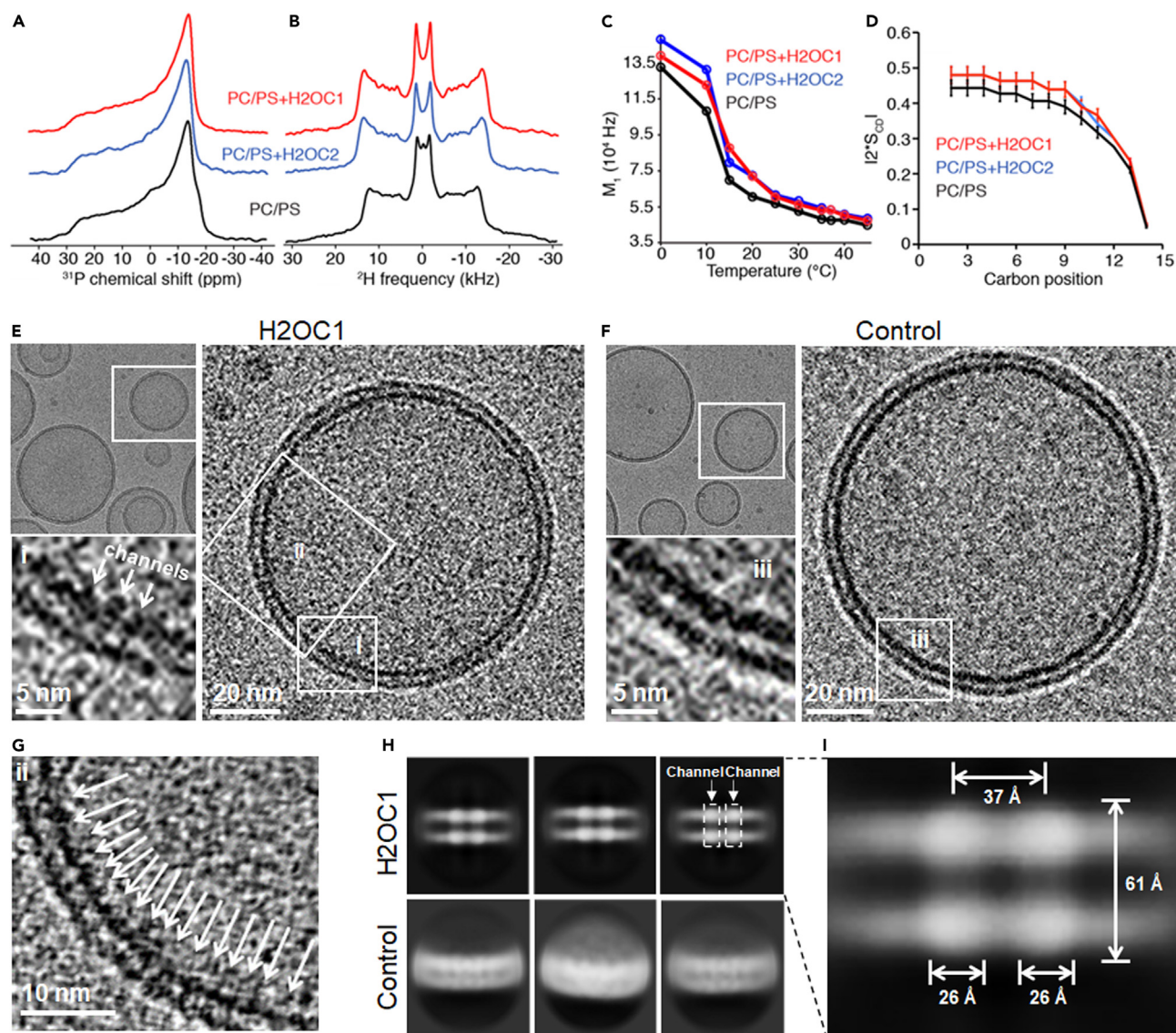


**Figure 2. Biophysical properties of foldamer insertion into liposomes and cryo-EM images of H2OC1-embedded PC/PS (4:1) liposomes**

(A)  $^{31}\text{P}$  static solid-state NMR experiments performed at 303 K on PC/PS control vesicles (black) and PC/PS vesicles incorporating H2OC1 (in red) and H2OC2 (in blue).

(B)  $^2\text{H}$  static solid-state NMR experiments performed at 303 K.

(C) Thermal variation of the first spectral moment  $M_1$  of PC lipids as measured by  $^2\text{H}$  solid-state NMR.

(D)  $\text{C}-^2\text{H}$  order parameter as a function of labeled lipid carbon position.

(E) Single particle cryo-EM image of self-assembled channels of H2OC1 in a liposome. The top left panel shows a low magnification image. Arrows point to three channels in the enlarged view (i) the boxed area (ii) showing an array of channels, see (G).

(F) Single particle cryo-EM image of control liposome without H2OC1. The magnified image shows a contiguous membrane without channels (iii).

(G) Magnified image shows the array of channels (arrows) in the lipid bilayer.

(H) Two-dimensional (2D) average images of H2OC1 EM particles (top). Two representative channels are outlined with dashed boxes. 2D averages of EM particle images of control liposomes (bottom); no obvious channel density was observed. For details, see [supplemental information](#).

(I) Size of each channel, the distance between two neighboring channels, and the membrane are indicated. The outer diameter of individual channels is 26 Å, compared with 29 Å in the crystal structure of H2OC1. The distance between two adjacent channels is 37 Å.

PC/PS liposomes stays the same in the presence of the H2OC1 and H2OC2 foldamers. Using spectral deconvolution, individual  $^2\text{H}$  quadrupolar splittings were employed to derive the lipid order parameters along the PC acyl chain (Figure 2D) that span half of a bilayer. Control PC/PS liposomes exhibited a characteristic profile

of  $S_{CD}$  order parameters with a plateau for carbons near the membrane surface and having a high structural order, followed by a decrease of order parameters toward the mobile methyl carbon C14. We observed a similar profile for liposomes incorporating H2OC1 and H2OC2, with a slight increase of  $S_{CD}$  order parameters in presence of the foldamers, suggesting that their insertion slightly increases lipid acyl chain ordering. Taken together, solid-state NMR experiments suggest a proper and stable insertion of foldamers into liposomes, without perturbations of the lipid phase, thermotropism, and internal dynamics.

Further, we employed single particle cryoelectron microscopy (cryo-EM) to estimate the number of H2OC1 channels within a unit area of the liposome membrane with an empty liposome as the control (Figures 2E–2G and S8). The cryo-EM image shows that the foldamer channels were inserted in an orderly fashion without perturbing the lipid phase. Under high magnification, rod-shaped densities corresponding to transmembrane channels were observed, which were absent in empty liposome images (Figures 2E and 2F). These channels are evenly distributed along the circular plane of the membrane (Figure 2G). Two-dimensional (2D) classification with a box size of 200 Å yielded average images of two channels embedded in the membrane (Figure 2H). By contrast, no corresponding dense regions were visible in the 2D averages of the empty liposome control (Figure 2H). The individual channels were 26 Å wide, consistent with the crystal structure (29 Å). Direct visualization of two neighboring channels allowed us to further measure their distance (Figure 2I), around 3.7 nm. Together, our cryo-EM analysis revealed that each H2OC1 channel occupies an area of 3.7 nm × 3.7 nm, which corresponds to 73,046 channels per  $\mu\text{m}^2$  at a 1:100 (foldamer to lipid) molar ratio.

### Water permeability of porin-type foldamer channels

We measured the water permeability in lipid bilayers using a stopped-flow method to capture fast kinetics on the millisecond time scale of water efflux from liposomes led by osmotic pressure difference was determined by monitoring the change in the light scattering intensity of the liposomes (Figure 3A).<sup>4,5,20,35,36</sup> We quantified the water permeability by the shrinkage mode, measured in PC/PS (4:1) liposomes. The foldamer-embedded liposomes were exposed to hypertonic osmolytes (sucrose and NaCl) (Figures 3A and 3B). The diameter of empty and foldamer-embedded liposomes was measured using light scattering intensity (Figure S9). Interestingly, all four foldamers showed significant water permeability in the presence of sucrose or competitive ionic NaCl used as osmolytes (Figures 3B, S9, and S10). H2OC1 and H2OC2 showed the highest water permeability compared with other sequences (5- to 7-fold increase in water transport at 1:50 ratio over the control vesicles without the foldamers) (Figure 3B). Additionally, these foldamer channels showed comparable water permeability to that of gramicidin A (gA),<sup>37</sup> a natural ionophore, which transports water and cations across the membranes (Figures 3B, S9, and S10).

The high water permeability of H2OC2 encouraged us to study the foldamer in more detail. Variation in lipid composition exhibits different properties of lipid membranes including charge, fluidity, and lateral pressure profiles.<sup>41</sup> Therefore, changes in lipid composition affect the interaction of lipids with extraneous compounds. The initial step of binding of a cationic molecule to anionic lipid PS-containing membranes occurs by electrostatic interactions.<sup>41</sup> Therefore, the effect of different PC/PS ratios in liposomes on water permeability of H2OC2 was evaluated (Figure S11). We observed no detectable water permeability in the presence of pure PC. However, with increasing PS concentration, the permeability increased until PC/PS ratio reached 4:1. Further

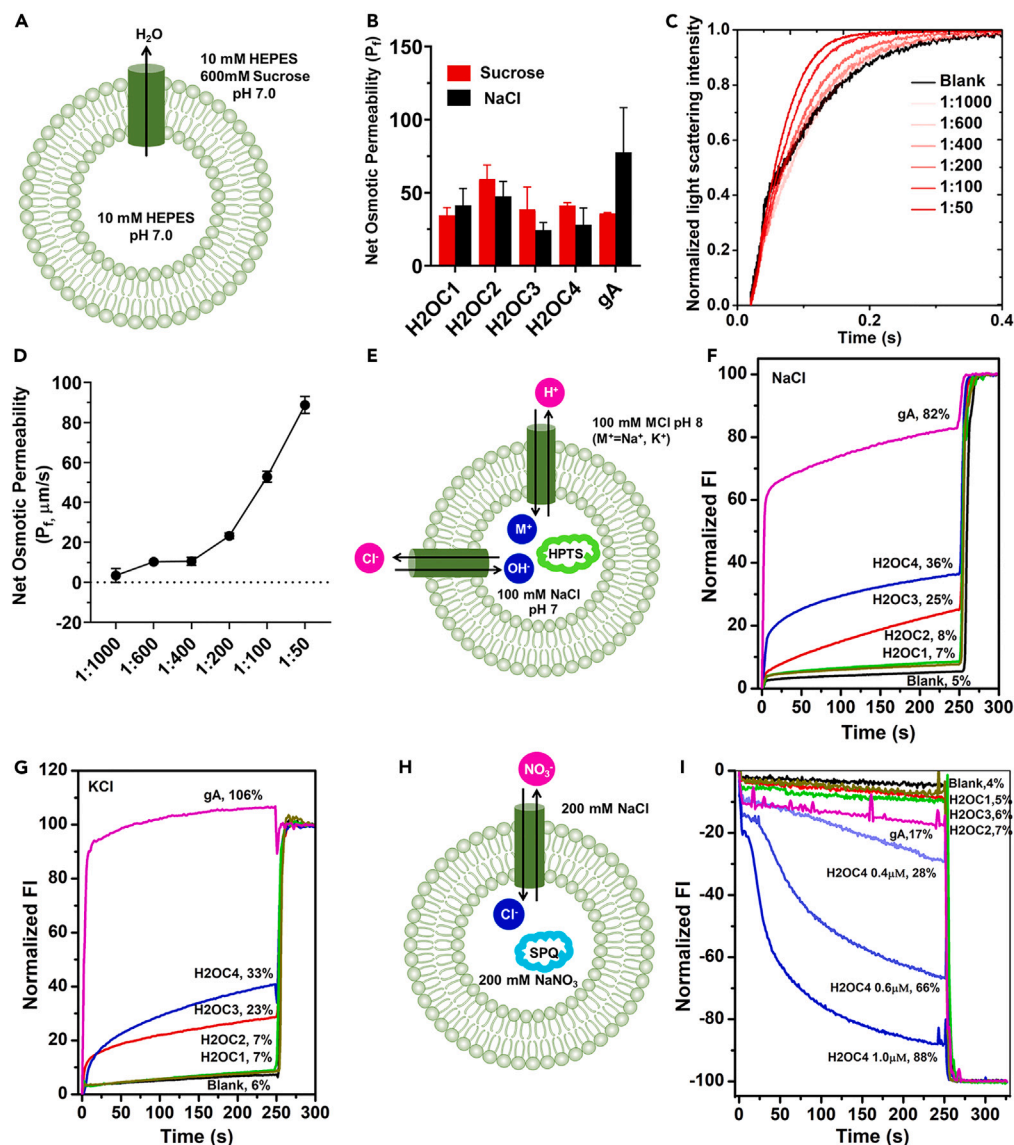


**Figure 3. Measurements of water and ion transport through oligoureia foldamers**

(A) Schematic representation of water permeability measurement through foldamer channels in phosphatidylcholine/phosphatidylserine (PC/PS) liposomes suspended in a hypertonic osmolyte (600 mM sucrose).

(B) Stopped-flow analysis of oligoureia foldamers showing water permeation through foldamer channels in PC/PS (4:1) liposomes. Data provided are mean  $\pm$  SE.

(C) Light scattering traces of H2OC2 embedded in PC/PS liposomes with different molar ratios showing an increasing water permeability with increased channel concentration when suspended in hypertonic osmolyte (600 mM sucrose). Curves were fitted with stretched function  $y = c + a \exp(-kx^b)$  to obtain exponential coefficients ( $k$ ).<sup>38–40</sup>

(D) Water permeability through the H2OC2 channel measured at different channel densities exhibited a jump in permeability when the lipid/channel molar ratio reached 100:1 to 50:1 indicating possible cooperativity. Data provided are mean  $\pm$  SE.

(E) Schematic representation of HPTS-based fluorescence assay under high ionic gradients (100 mM NaCl and KCl). HPTS, 8-hydroxypyrene-1,3,6-trisulfonic acid.

(F and G) Salt rejections by H2OC1 and H2OC2 compared with natural ionophore gramicidin A (gA) and foldamers H2OC3 and H2OC4.

(H) Schematic representation of chloride-selective, SPQ dye-based, fluorescence assay for ion transport.

(I) Chloride-selective ion transport by SPQ fluorescence quenching assay showed rejection of chloride ion by H2OC1, H2OC2, and H2OC3. Concentration-dependent fluorescence quenching was observed with H2OC4, indicating chloride transport by H2OC4.

increase in PS concentration for H2OC2 resulted in decreased water permeability (Figure S11). The 10-residue oligourea foldamers consist of polar Lys<sup>U</sup> and Glu<sup>U</sup> residues. The ionic nature of these residues facilitates binding to membranes through electrostatic interactions. Further, the inclusion of anionic lipid PS in the membrane increases the electrostatic interactions with the foldamers. The insertion of foldamers in the membrane is further facilitated by their external hydrophobic surface.

Subsequently, H2OC2 and PC/PS liposomes were mixed to obtain foldamer/lipid molar ratios from 1:1,000 to 1:50 in 10 mM HEPES buffer, pH 7.0, and measured their water permeability.

The light scattering intensity increased with exposure to an equal volume of hypertonic osmolyte (600 mM sucrose) with the increasing foldamer ratio (Figures 3C and 3D). This indicates that increasing the molar ratio results in an effective increase in the incorporation of foldamers into the liposomes, leading to enhanced water permeation. The calculated water permeability ( $P_f$ ) values of H2OC2 vary from 10.5  $\mu\text{m/s}$  (foldamer/lipid 1:400), 23.2  $\mu\text{m/s}$  (@1:200) to 88.7  $\mu\text{m/s}$  (@1:50) (Figures 3C and 3D), close or superior to water permeability observed with gA channels. H2OC2 also showed water permeability in the presence of other osmolytes such as glycine and glucose (Figure S12). Furthermore, the water permeability at pH 4.5 was lower than that at pH 7.0.

From the cryo-EM data, we calculated the channel number to be  $\sim 1,665$  per liposome (for a 1:100 molar ratio where 135  $\mu\text{M}$  of H2OC1 was used in 13,500  $\mu\text{M}$  PC/PS). The net osmotic permeability ( $P_f$ ) of H2OC1 was calculated as 34.44  $\mu\text{m/s}$  (for details see supplemental information). Thus, the calculated single-channel water permeability of H2OC1 was  $P_1 = 8.08 \times 10^{-16} \text{ cm}^3/\text{s}$ ; and  $P_2 = 2.70 \times 10^7$  water molecules/s. If we presume that H2OC2 will form a similar channel assembly as that of H2OC1 due to their sequence similarities, the inserted channel numbers in PC/PS membranes are also expected to be similar. The net osmotic permeability ( $P_f$ ) of H2OC2 was calculated as 52.82  $\mu\text{m/s}$  (for details see Figures S10–S12). Therefore, the estimated single-channel permeability of H2OC2 was  $P_1 = 1.21 \times 10^{-15} \text{ cm}^3/\text{s}$ ; and  $P_2 = 4.08 \times 10^7$  water molecules/s.

### Proton/ion transport properties of foldamers

High selective water transport is the most important feature for an AWC. Another crucial feature that is equally important for water purification is its ability to reject ion transport.<sup>42,43</sup> Therefore, we determined the ion transport properties of our selected foldamers in PC/PS (4:1) liposomes using a standard fluorescence-based 8-hydroxypyrene-1,3,6-trisulfonic acid (HPTS) assay (Figure 3E). The HPTS-loaded liposomes were incubated with the foldamers for 5 min. before the experiments. A base pulse (20  $\mu\text{L}$  of 0.5 N NaOH) was given at 50 s of the measurement to increase the external pH from 7.0 to 8.0. The natural ionophore gA, a monovalent cation selective channel<sup>37</sup> was used as a positive control (Figures 3F and 3G). The changes in fluorescence intensity showed that H2OC3 (36%) and H2OC4 (25%) channels can moderately transport  $\text{Na}^+$  and  $\text{K}^+$  ions. However, the ion transport facilitated by the foldamers was much lower than that of gA (Figures 3F and 3G). Interestingly, no detectable ion transport activity was observed for H2OC1 (7%) and H2OC2 (8%) in the presence of NaCl and KCl (Figures 3F and 3G). In addition, H2OC1 and H2OC2 foldamers are able to reject the divalent ions (Figure S13). This indicates the strong salt rejection ability of these two foldamers. Therefore, they are suitable for water purification applications.

The chloride permeation through H2OC1 and H2OC2 channels was further investigated using chloride-selective dye 6-methoxy-N-(3-sulfopropyl)quinolinium (SPQ)<sup>42,43</sup> trapped in PC/PS (4:1) liposomes containing intravesicular NaNO<sub>3</sub> and extravesicular NaCl (Figure 3H). Oligourea H2OC1, H2OC2, and H2OC3 did not show any detectable chloride transport (Figure 3I). However, concentration-dependent quenching of fluorescence intensity was observed for H2OC4 due to the influx of Cl<sup>-</sup> ions (Figure 3I). Collectively, these assays confirm the ion rejection properties of H2OC1 and H2OC2.

The proton transport activity of oligourea foldamers was evaluated by the patch-clamp experiments<sup>20,29</sup> in PC:PS (4:1) and 1,2-dioleoyl-sn-glycero-3-phosphocholine (DOPC) liposomes (Figures S14–S18).<sup>37</sup> The proton conductance rates of H2OC1 ( $\gamma_{H^+} = 7.4$  pS) and H2OC2 ( $\gamma_{H^+} = 25.8$  pS) showed differences in PC:PS liposomes (Figure S14), but the values did not differ significantly in DOPC liposomes (Figure S15). H2OC1 presents a better channel shape, longer retention time, and higher channel opening probability at both lipid conditions (Figures S14 and S15). Along with the water transport activity, we can speculate that protons are transferred overall along water wires. Patch-clamp single-channel current traces and I-V plots of H2OC1 and H2OC2 recorded in symmetrical solutions (*cis* chamber = *trans* chamber = 1 M KCl solution) and asymmetrical solutions (*cis* chamber = 1 M KCl solution, *trans* chamber = 1 M NaCl solution) using DOPC and PC/PS (4:1) lipids show no obvious channel activity confirming the previously observed lack of ion transport ability by H2OC1 (Figures S16 and S18A) and H2OC2 (Figures S17 and S18B). H2OC1 and H2OC2 showed extremely low channel current (<5  $\mu$ A). The observed channel opening under high voltage could have occurred due to ion polarization, which is not characteristic of ion transporters.<sup>44–46</sup> Hence, the calculation of single-channel ion permeability is not feasible here.

### Self-assembled channel structure of foldamer

An X-ray crystal structure of foldamer H2OC1 at a high resolution of 1.2 Å was determined in order to provide atomic-scale details of channel formation via self-assembly (Figures 4 and S19–S22; Tables S2 and S3). The monomers exhibit the design-imposed amphipathic helical conformation consisting of distinct hydrophobic and hydrophilic faces (Figures 1A and 4A) similar to those formed from H2 (Figure S19; Table S3).<sup>23</sup> Crystal packing revealed oligourea helices forming a self-assembled superhelical channel-type assembly (Figure 4B).

Two distinct channels can be identified in the crystal structure of H2OC1, namely channels A and B with an external diameter of 29 Å each (Figure 4B), which is close to the dimensions observed in the cryo-EM images. These channels show apparent pore diameters of 4.8 and 6.4 Å, respectively. In channel B, the electron density maps for C-terminal Lys<sup>U</sup>9, and Ala<sup>U</sup>10 residues are not “visible,” leading to the overestimation of its pore size. In both channels, the exterior surface is composed of the hydrophobic residues Leu<sup>U</sup>, Ala<sup>U</sup>, and Pro<sup>U</sup> located at positions a, c, and e in the helical-wheel representation. The pore of the channels is lined by the hydrophilic residues Glu<sup>U</sup> and Lys<sup>U</sup> situated at positions b and d (Figure 4B). Eight oligourea helices per turn associate laterally in a right-handed, staggered, antiparallel orientation by hydrophobic and electrostatic interactions within the superhelical structure. The intricate H-bonding network of salt bridges between neighboring oligourea helices greatly contributes to stabilizing the pore structure. The hydrophilic pore is hydrated with both H-bonded (to the Glu<sup>U</sup> and Lys<sup>U</sup> side chains) and mobile water molecules (Figures 4C, 4D, S20, and S21). A single turn (23 Å) could span across half the thickness of phospholipid bilayers. Interestingly, the crystal packing

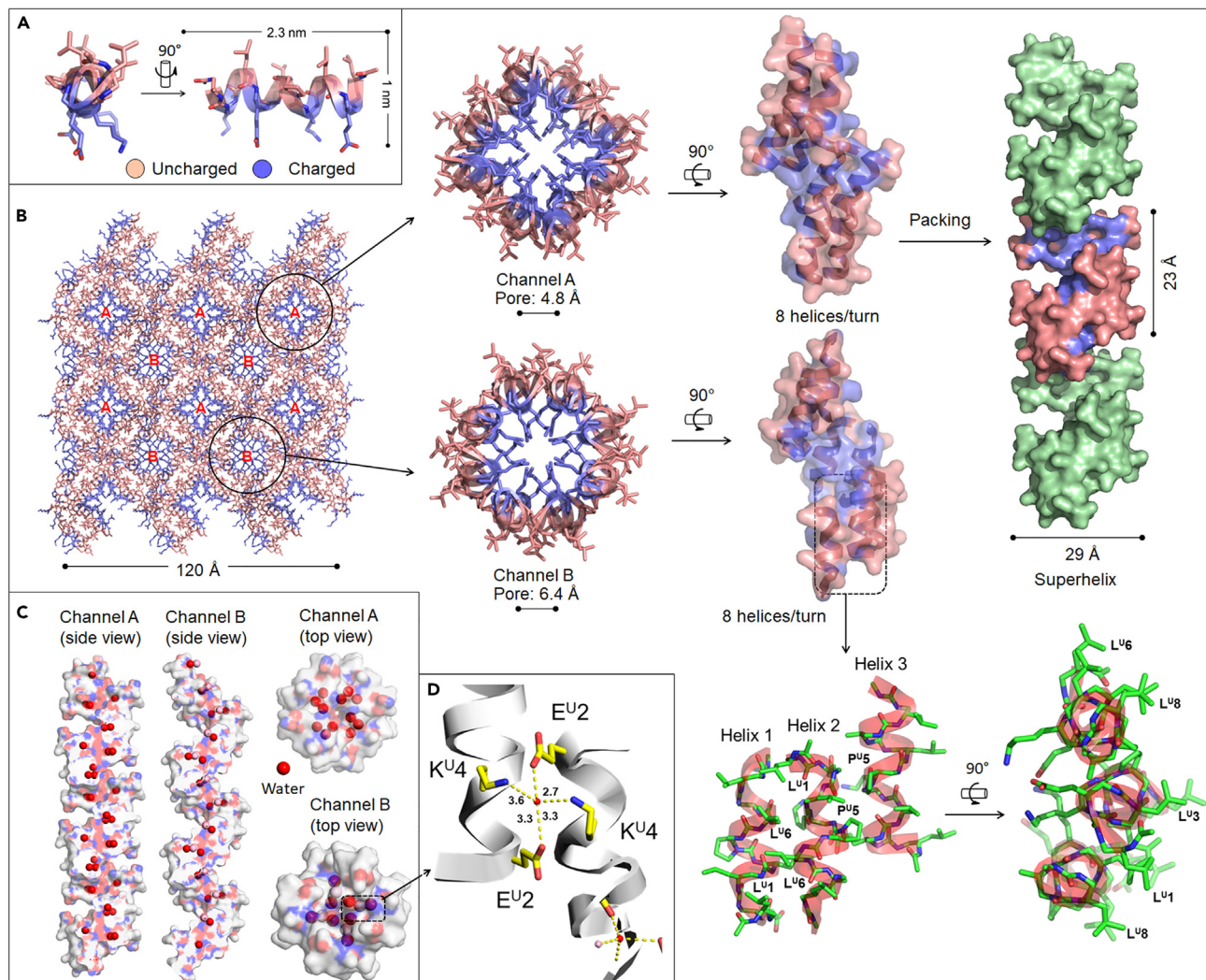


**Figure 4. Crystal structure revealing the quaternary structure of foldamer H2OC1**

(A) Crystal structure of H2OC1 shows a helical conformation of the monomer with distinct hydrophobic (salmon red) and hydrophilic (blue) surfaces. (B) Crystal packing shows two distinct channels (channel A and channel B). In this structure, channel B is formed in the interspace of four channel A assemblies. Both channels are packed through hydrophobic interactions of exterior surfaces. In the channel assembly, eight monomeric oligoureia helices per turn are packed laterally. The neighboring helices are in an antiparallel orientation within the superhelical structure that has an outer diameter of 29 Å. Each turn of this superhelical assembly spans 23 Å. The interiors of both channels are composed of hydrophilic residues, creating a charged nanopore, while hydrophobic residues line the exterior. (C) Water molecules that are H-bonded with the foldamer are shown as red spheres in the pores of channels A and B. Water molecules that do not form any H-bonding with foldamer helices are represented as pink spheres. Only selected water molecules are displayed. (D) Water molecules in the pore form a H-bonding network with charged residues, Glu<sup>U</sup> and Lys<sup>U</sup>. Hydrogen bonds show O–O and N–O distances of 2.7 and 3.6 Å, respectively. Images were created using PyMOL.

also revealed the presence of distorted helices that fill the void spaces between channel assemblies. These helices with a kink near the Pro<sup>U</sup> and Lys<sup>U</sup> residues are situated externally, defining four corners surrounding both channel assemblies (Figure S22). The well-defined self-assembled helical tubular structure of H2OC1 in the crystal (Figure 4B) may suggest a model of interaction between the hydrophobic face of amphipathic foldamer helices and the hydrophobic component of lipid membranes compatible with the formation of a pore in the lipid membranes. Based on such a mode, one hypothesis could be that water transport across the membranes occurs via the H-bonding networks between water molecules and the hydrophilic

residues in the pore wall (Figures 4C and 4D). TEM analysis of H2OC1 under conditions similar to those of crystallization revealed an extended fiber assembly with an external diameter of about 20.6 nm (Figure S23A). These fibers may be formed of five- to six-channel units across their diameter. By contrast, H2OC2 fiber bundles are about 9.3 nm in diameter (Figure S23B).

### All-atom molecular dynamics (MD) simulations

To gain molecular insights into the dynamics of the H2OC1 channel in the lipid bilayer, we performed explicitly solvated all-atom MD simulations. We used the experimental crystal structure of the H2OC1 channel composed of 8 monomeric helices as well as 16 kinked H2OC1 oligourea helices positioned on the side of the channel. We embedded this construct in a POPC: POPS (4:1 ratio; POPC [1-palmitoyl-2-oleoyl-sn-glycero-3-phosphocholine], POPS [palmitoyl-oleoyl PS]) lipid bilayer (Figure 5Ai). After 200 ns of the equilibration simulation with restrained alpha carbon positions of all helical oligoureas only, we observed that 12 kinked peptides that were positioned between lipid head groups of the membrane remained bound to the channel (Figure 5Aii), whereas those above or below dissociated.

After 600 ns of the unrestrained production run, the channel retained its supra helical conformation (Figures 5Aiii; Videos S1 and S2) with kinked peptides bound. We also built a control system, which corresponded to the H2OC1 channel composed only of 8 monomeric helices in the same lipid environment (Figure 5Biv). After 200 ns equilibration and 600 ns of the production, the supra helix collapsed resembling a closed and cylindrical conformation (Figure 5Bv; Videos S3 and S4). This is indicated by a higher root-mean-square deviation (RMSD) of alpha carbons for the system without kinked helices (Figure 5D). Although water molecules were found to permeate through both channels, the H2OC1 channel with kinked peptides could transport better water molecules (Figure 5D). The longer permeation pathway of the H2OC1 channel with kinked helices allowed the formation of more hydrogen bonds between two glutamate-type residues in each oligourea with water molecules (Figures S24A and S24B). On the other hand, a small fraction of ions could enter both channels, in agreement with our experimental observations (Figures 2E–2I). Averaged radius profiles as well as averaged density of solvent in both channels are shown in Figures 5F and 5G. Although both channels have a radius in the membrane center of mass corresponding to ~0.2 nm, indeed, the H2OC1 channel with kinked peptides has a significantly longer permeation pathway. In summary, computer simulations showed that kinked peptides can stabilize the H2OC1 channel, which allows more water molecules to permeate through the membrane.

### Conclusions

We have successfully designed and synthesized oligourea foldamers that form superhelical water channels in aqueous conditions stabilized by hydrophobic and electrostatic interactions. Oligourea foldamers H2OC1 and H2OC2 showed significant water permeability with high salt rejection in liposomes. By contrast, H2OC3 and H2OC4 showed permeability to ions along with water in liposomes. A high-resolution crystal structure of H2OC1 revealed that salt bridges facilitate intricate H-bonding networks among proximal and distal oligourea residues to stabilize the packing, which was confirmed by the formation of fibers of the same dimension that were observed by TEM. Solid-state NMR and cryo-EM data suggest the stable insertion of foldamers without perturbing the liposomes. The design of the amphiphilic foldamers results in the formation of self-assembled tertiary structures conferring a hydrophobic exterior and hydrophilic interior lumen filled with H-bonded water clusters. It results in high water permeability across lipid

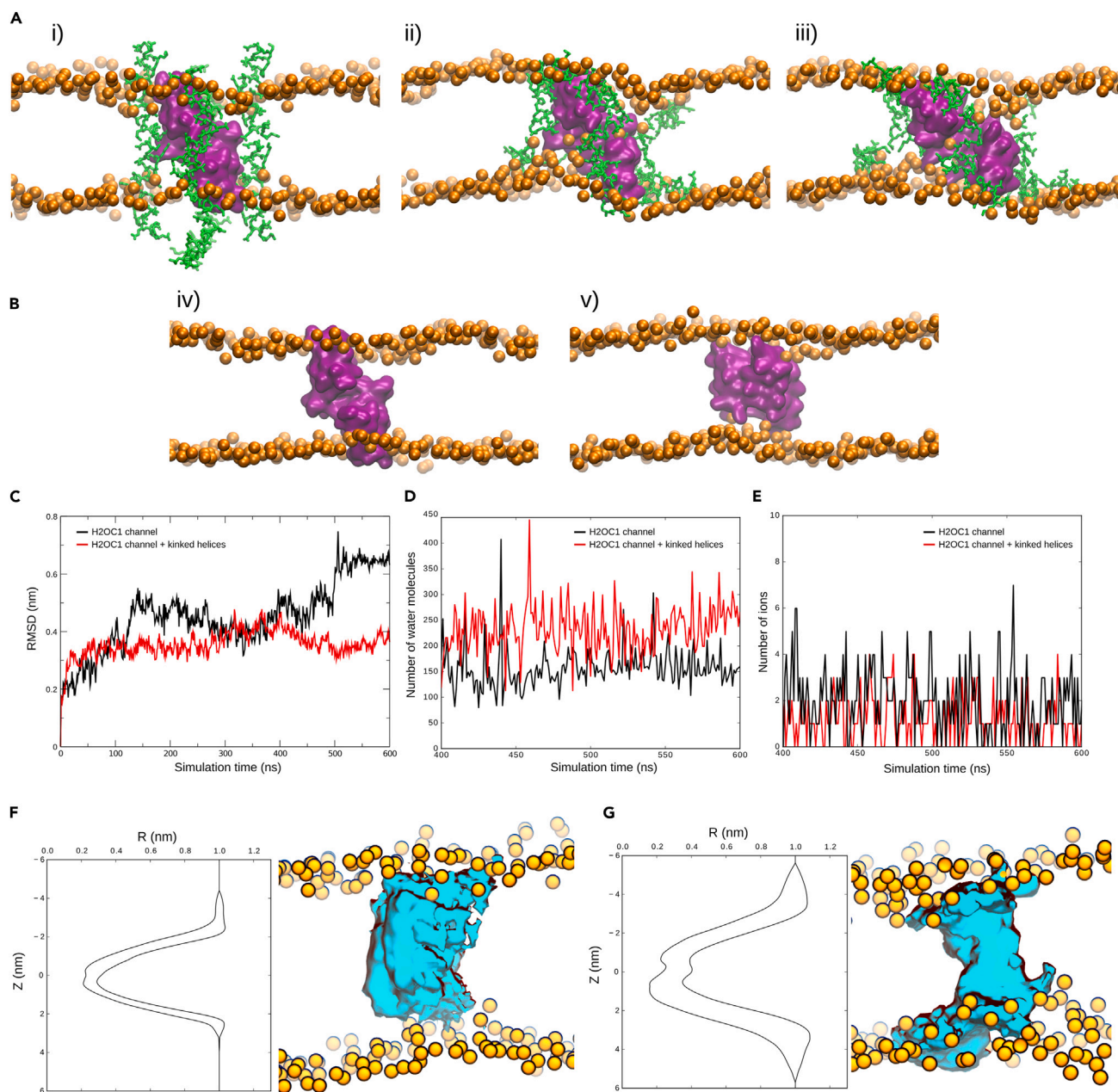


**Figure 5. Molecular dynamics simulations of H2OC1 oligoureia channel in POPC:POPS (4:1 ratio) lipid bilayer**

(A) The H2OC1 oligoureia channel composed of 8 helical and 16 kinked helices embedded in lipid bilayer together with simulation snapshots: (i) prior to any simulation, (ii) after 200 ns of equilibration with position restraints on helical foldamer alpha carbon atoms, and (iii) after 600 ns of the production run without any restraints. The surface representation of the helices is shown in purple. The 16 kinked helices are shown in green licorice representation. Orange spheres correspond to phospholipid head groups. Water, ions, and lipid headgroups were omitted for figure clarity.

(B) Control system of the H2OC1 oligoureia channel composed of 8 helices alone together with simulation snapshots: (iv) after 200 ns of equilibration with position restraints on alpha carbon atoms and (v) after 600 ns of the production run without any restraints.

(C) Root mean-square-deviation (RMSD) of alpha carbon atoms from 8 helices calculated with respect to the experimental structure.

(D and E) Number of water molecules (D) and the number of ions (E) passing through both channel types (shown in A and B) over the last 200 ns of the trajectory are shown.

(F and G) Average channel radius profile across the membrane normal (the two radius profile tracings in each represent the standard deviation limits) together with snapshots of the averaged density of the solvent within the pore (blue) are shown for the two cases, namely, with (F) and without (G) helices. The radius profile, as well as solvent density, were averaged over the last 200 ns of the production run.

membranes. Therefore, such oligourea foldamers that are similar to natural porin-like structures are potential candidates for the fabrication of AWC membranes for water purification applications.

Unlike the previously described AWCs, our foldamers laterally self-assemble to form the channel. This represents a novel design strategy of using short (10-residue) oligourea foldamers for AWCs and other channels/transporters. We could achieve distinct water and ion permeabilities by altering the sequences of foldamers. The *de novo* design described herein has potential advantages. Changing the hydrophobic and hydrophilic surfaces of these foldamers allows the self-assembly of channels with different diameters and water/ion permeabilities. The design strategy of incorporating polar and nonpolar side chains within the channel lumen could allow selective interactions and transport of cations, anions, and water. This highlights the versatility and potential of such oligourea foldamers for systematic and rational design to achieve different structural and functional properties.

## EXPERIMENTAL PROCEDURES

### Resource availability

#### Lead contact

Further information and requests for resources and reagents should be directed to and will be fulfilled by the lead contact, Prakash P. Kumar ([prakash.kumar@nus.edu.sg](mailto:prakash.kumar@nus.edu.sg)) and Gilles Guichard ([g.guichard@iecb.u-bordeaux.fr](mailto:g.guichard@iecb.u-bordeaux.fr)).

#### Materials availability

Unique reagents generated in this study are available from the lead contact with a completed material transfer agreement.

#### Data and code availability: Structure determination by X-ray crystallography

All relevant data are provided in the main text and [supplemental information](#), and there are no codes generated uniquely for this study. The CCDC code for the crystal structure of foldamer H2OC1 is: 2211250, and the data collection and refinement statistics for the X-ray crystal structure are provided in [Table S2](#).

### Solid phase synthesis of oligourea foldamers

Oligourea foldamers H2OC1, H2OC2, H2OC3, and H2OC4 were synthesized by standard solid phase peptide synthesis methods using azide chemistry according to previously reported procedures.<sup>23,26</sup> After synthesis, the foldamers were purified by reversed-phase high-performance liquid chromatography (RP-HPLC) using C<sub>18</sub> column prior to characterization by MS and analytical RP-HPLC.

### Transmission electron microscopy (TEM)

Foldamer samples (200  $\mu$ M in 10 mM HEPES pH 7.0) were deposited on carbon-coated copper grid and subjected to negative staining with 2% uranyl acetate. The conformations of various foldamers were observed under JEOL 1400Flash TEM.

### Studies of foldamer-phospholipid interaction using solid-state NMR

Foldamers H2OC1 and H2OC2 were added to liposomes (DMPC-d<sub>54</sub> and POPS at 4:1 molar ratio) at foldamer:lipid ratio of 1:20. A quadrupolar spin-echo sequence was applied at a <sup>2</sup>H frequency of 76.8 MHz on a 500 MHz (11.7 T) Bruker Avance III NMR spectrometer for <sup>2</sup>H static wide-line solid-state NMR experiments. Further, a Hahn-echo sequence was applied at a <sup>31</sup>P frequency of 161.9 MHz on a 400 MHz (9.4 T) Bruker Avance III HD NMR spectrometer for <sup>31</sup>P static wide-line

solid-state NMR. Control data were obtained with lipids without foldamers. Data were acquired at different temperatures (273–318 K).

### Single particle cryo-EM to determine insertion of H2OC1 channels into lipid vesicles

Liposome samples with or without H2OC1 on glow-discharged Quantifoil holey gold grids (R 1.2/1.3, Cu 400 mesh) were plunge-frozen in liquid ethane cooled by liquid nitrogen (FEI Vitrobot System). Cryo-EM data were collected as 34-frame movies (130,000 $\times$  magnification)<sup>47</sup> on a Titan Krios electron microscope (Thermo Fisher Scientific). Data were processed using CryoSPARC.<sup>48</sup> 2D averages of selected particles (37,219 particles of H2OC1 and 41,535 particles from empty liposomes picked by “Blob picker” after “patch CTF estimation”) were obtained by running “2D classification” in CryoSPARC.<sup>48–50</sup> The number of channels per liposome was calculated based on the dimensions of the liposomes and channels as described in the [supplemental information](#).

### Water transport assay by stopped-flow method

The water permeability was measured using PC:PS (4:1 molar ratio) liposomes with various foldamers (1:100 molar ratio) on a stopped-flow instrument (Chirascan circular dichroism spectrometer, Applied Photophysics, UK).<sup>51</sup> The liposomes were exposed to hypertonic osmolytes (600 mM sucrose) leading to shrinkage due to water efflux.

### Measurements of ion transport activity

The ion transport activities of the foldamers were measured in PC:PS liposomes (4:1 molar ratio) containing pH-sensitive HPTS (1 mM) dye using Shimadzu RF-6000 fluorescence spectrophotometer.<sup>42,43</sup> Similarly, chloride-selective transport was measured using SPQ dye.<sup>42,43</sup>

### Single-channel current measurement using planar lipid bilayer workstation

Planar lipid bilayers were formed by brushing 0.2  $\mu$ L of 4:1 PC:PS- or DOPC-containing n-decane around the aperture. Single-channel current traces (proton or ion transport) were tested at different voltages using patch-clamp techniques.<sup>37,51</sup>

### Structure determination by X-ray crystallography

H2OC1 (10 mg/mL in water) were crystallized using sparse-matrix screening kits (Cation suite [Nextal] and Proplex [Molecular Dimensions]) in 96-well plates by sitting-drops method. Crystals were optimized in 24-well plates with the hanging drops method at room temperature as well as at 16°C. Diffraction-quality crystals of H2OC1 were obtained (0.1 M HEPES pH 7.5, 0.2 M ammonium acetate plus 15% v/v isopropanol). X-ray diffraction data were collected on beamline 23-ID-D at the Advanced Photon Source, Argonne National Laboratory and analyzed as described earlier.<sup>23</sup> The massiveness of this structure prevents typical small-molecule X-ray crystallography analysis in detail. Please refer to [supplemental information](#) for detailed [experimental procedures](#), and [Data S1](#) and [S2](#) for the raw data.

## SUPPLEMENTAL INFORMATION

Supplemental information can be found online at <https://doi.org/10.1016/j.chempr.2023.04.007>.

## ACKNOWLEDGMENTS

This research was supported by the National Research Foundation Singapore and PUB, Singapore’s National Water Agency under its Competitive Research

Programme, CRP (Water) (1601-CRPW-T21). G.G. and M.B. acknowledge support from the CNRS through the MITI interdisciplinary programs (Défi Biomimetisme 2019, 2020). This work was also partly supported by the Agence Nationale de la Recherche (ANR) grants ANR-17-CE07-0020 and ANR-18-CE06-0004-02, WATERCHANNELS. A postdoctoral fellowship to S.H.Y from IdEx Bordeaux (ANR-10-IDEX-03-02), a program of the French government managed by the ANR, is gratefully acknowledged. This work has benefited from the Biophysical and Structural Chemistry Platform at IECB, CNRS UAR 3033, INSERM US001. Mr. Choong Yeu Khai provided technical help with the X-ray data collection. D.S. appreciates receiving a scholarship from China Scholarship Council as support at the University of Montpellier, France.

### AUTHOR CONTRIBUTIONS

G.G., R.M.K., P.P.K., and C.D. devised the project. C.D., G.G., S.H.Y., M.P., and P.K. designed and synthesized the molecular structures at IECB, France, and carried out the experimental work. C.D. obtained the crystals and diffraction data. G.W.C. solved and refined the crystal structure. A.L. and A.G. designed and performed solid-state NMR (ssNMR) experiments. J.L. and M.L. performed cryo-EM studies. D.S. and M.B. carried out patch-clamp work and verified liposome assays. J.K.M., P.J.B., and C.V. carried out the MD simulation work. C.D., G.G., G.W.C., A.L., M.B., R.M.K., and P.P.K. analyzed the experimental data. All authors participated in manuscript writing and editing. Funding acquisition and supervision by G.G., M.B., R.M.K., and P.P.K.

### DECLARATION OF INTERESTS

C.D., P.K., D.S., S.H.Y., G.G., M.B., R.M.K., and P.P.K. are inventors on a patent application related to this work (Singapore Patent Application no. 10202300606Y, filed on 07 March 2023).

Received: November 4, 2022

Revised: February 6, 2023

Accepted: April 11, 2023

Published: May 8, 2023

### REFERENCES

- Porter, C.J., Werber, J.R., Zhong, M., Wilson, C.J., and Elimelech, M. (2020). Pathways and challenges for biomimetic desalination membranes with sub-nanometer channels. *ACS Nano* 14, 10894–10916. <https://doi.org/10.1021/acsnano.0c05753>.
- Barboiu, M., and Gilles, A. (2013). From natural to bioassisted and biomimetic artificial water channel systems. *Acc. Chem. Res.* 46, 2814–2823. <https://doi.org/10.1021/ar400025e>.
- Murata, K., Mitsuoka, K., Hirai, T., Walz, T., Agre, P., Heymann, J.B., Engel, A., and Fujiyoshi, Y. (2000). Structural determinants of water permeation through aquaporin-1. *Nature* 407, 599–605. <https://doi.org/10.1038/35036519>.
- Yuan, Y.D., Dong, J., Liu, J., Zhao, D., Wu, H., Zhou, W., Gan, H.X., Tong, Y.W., Jiang, J., and Zhao, D. (2020). Porous organic cages as synthetic water channels. *Nat. Commun.* 11, 4927. <https://doi.org/10.1038/s41467-020-18639-7>.
- Tunuguntla, R.H., Henley, R.Y., Yao, Y.C., Pham, T.A., Wanunu, M., and Noy, A. (2017). Enhanced water permeability and tunable ion selectivity in subnanometer carbon nanotube porins. *Science* 357, 792–796. <https://doi.org/10.1126/science.aan2438>.
- Li, Y., Li, Z., Aydin, F., Quan, J., Chen, X., Yao, Y.C., Zhan, C., Chen, Y., Pham, T.A., and Noy, A. (2020). Water-ion permselectivity of narrow-diameter carbon nanotubes. *Sci. Adv.* 6, eaba9966. <https://doi.org/10.1126/sciadv.aba9966>.
- Le Duc, Y., Michau, M., Gilles, A., Gence, V., Legrand, Y.M., van der Lee, A., Tingry, S., and Barboiu, M. (2011). Imidazole-quartet water and proton dipolar channels. *Angew. Chem. Int. Ed. Engl.* 50, 11366–11372. <https://doi.org/10.1002/anie.201103312>.
- Licsandru, E., Kocsis, I., Shen, Y.X., Murail, S., Legrand, Y.M., Van Der Lee, A., Tsai, D., Baaden, M., Kumar, M., and Barboiu, M. (2016). Salt-excluding artificial water channels exhibiting enhanced dipolar water and proton translocation. *J. Am. Chem. Soc.* 138, 5403–5409. <https://doi.org/10.1021/jacs.6b01811>.
- Huang, L.B., Di Vincenzo, M., Ahunbay, M.G., Van Der Lee, A., Cot, D., Cerneaux, S., Maurin, G., and Barboiu, M. (2021). Bilayer versus polymeric artificial water channel membranes: structural determinants for enhanced filtration performances. *J. Am. Chem. Soc.* 143, 14386–14393. <https://doi.org/10.1021/jacs.1c07425>.
- Di Vincenzo, M., Tiraferrri, A., Musteata, V.E., Chisca, S., Sougrat, R., Huang, L.B., Nunes, S.P., and Barboiu, M. (2021). Biomimetic artificial water channel membranes for enhanced desalination. *Nat. Nanotechnol.* 16, 190–196. <https://doi.org/10.1038/s41565-020-00796-x>.
- Itoh, Y., Chen, S., Hirahara, R., Konda, T., Aoki, T., Ueda, T., Shimada, I., Cannon, J.J., Shao, C., Shiomi, J., et al. (2022). Ultrafast water permeation through nanochannels with a densely fluorinated interior surface. *Science* 376,

- 738–743. <https://doi.org/10.1126/science.abd0966>.
12. Hu, X.B., Chen, Z., Tang, G., Hou, J.L., and Li, Z.T. (2012). Single-molecular artificial transmembrane water channels. *J. Am. Chem. Soc.* **134**, 8384–8387. <https://doi.org/10.1021/ja302292c>.
13. Shen, Y.X., Si, W., Erbakan, M., Decker, K., De Zorzi, R., Saboe, P.O., Kang, Y.J., Majd, S., Butler, P.J., Walz, T., et al. (2015). Highly permeable artificial water channels that can self-assemble into two-dimensional arrays. *Proc. Natl. Acad. Sci. USA* **112**, 9810–9815. <https://doi.org/10.1073/pnas.1508575112>.
14. Song, W., Joshi, H., Chowdhury, R., Najem, J.S., Shen, Y.X., Lang, C., Henderson, C.B., Tu, Y.M., Farrell, M., Pitz, M.E., et al. (2020). Artificial water channels enable fast and selective water permeation through water-wire networks. *Nat. Nanotechnol.* **15**, 73–79. <https://doi.org/10.1038/s41565-019-0586-8>.
15. Lang, C., Deng, X., Yang, F., Yang, B., Wang, W., Qi, S., Zhang, X., Zhang, C., Dong, Z., and Liu, J. (2017). Highly selective artificial potassium ion channels constructed from pore-containing helical oligomers. *Angew. Chem. Int. Ed. Engl.* **56**, 12668–12671. <https://doi.org/10.1002/anie.201705048>.
16. Zhu, J., Dong, Z., Lei, S., Cao, L., Yang, B., Li, W., Zhang, Y., Liu, J., and Shen, J. (2015). Design of aromatic helical polymers for STM visualization: imaging of single and double helices with a pattern of  $\pi$ - $\pi$  stacking. *Angew. Chem. Int. Ed. Engl.* **54**, 3097–3101. <https://doi.org/10.1002/anie.201410975>.
17. Lang, C., Li, W., Dong, Z., Zhang, X., Yang, F., Yang, B., Deng, X., Zhang, C., Xu, J., and Liu, J. (2016). Biomimetic transmembrane channels with high stability and transporting efficiency from helically folded macromolecules. *Angew. Chem. Int. Ed. Engl.* **55**, 9723–9727. <https://doi.org/10.1002/anie.201604071>.
18. Huo, Y., and Zeng, H. (2016). “Sticky”-ends-guided creation of functional hollow nanopores for guest encapsulation and water transport. *Acc. Chem. Res.* **49**, 922–930. <https://doi.org/10.1021/acs.accounts.6b00051>.
19. Shen, J., Fan, J., Ye, R., Li, N., Mu, Y., and Zeng, H. (2020). Polypyridine-based helical amide foldamer channels: rapid transport of water and protons with high ion rejection. *Angew. Chem. Int. Ed. Engl.* **59**, 13328–13334. <https://doi.org/10.1002/anie.202003512>.
20. Roy, A., Shen, J., Joshi, H., Song, W., Tu, Y.M., Chowdhury, R., Ye, R., Li, N., Ren, C., Kumar, M., et al. (2021). Foldamer-based ultrapermeable and highly selective artificial water channels that exclude protons. *Nat. Nanotechnol.* **16**, 911–917. <https://doi.org/10.1038/s41565-021-00915-2>.
21. Shen, J., Roy, A., Joshi, H., Samineni, L., Ye, R., Tu, Y.M., Song, W., Skiles, M., Kumar, M., Aksimentiev, A., and Zeng, H. (2022). Fluorofoldamer-based salt- and proton-rejecting artificial water channels for ultrafast water transport. *Nano Lett.* **22**, 4831–4838. <https://doi.org/10.1021/acs.nanolett.2c01137>.
22. Yoo, S.H., Li, B., Dolain, C., Pasco, M., and Guichard, G. (2021). Urea based foldamers. *Methods Enzymol.* **656**, 59–92. <https://doi.org/10.1016/bs.mie.2021.04.019>.
23. Collie, G.W., Pulka-Ziach, K., Lombardo, C.M., Fremaux, J., Rosu, F., Decossas, M., Mauran, L., Lambert, O., Gabelica, V., Mackereth, C.D., and Guichard, G. (2015). Shaping quaternary assemblies of water-soluble non-peptide helical foldamers by sequence manipulation. *Nat. Chem.* **7**, 871–878. <https://doi.org/10.1038/nchem.2353>.
24. Yoo, S.H., Collie, G.W., Mauran, L., and Guichard, G. (2020). Formation and modulation of nanotubular assemblies of oligourea foldamers in aqueous conditions using alcohol additives. *ChemPlusChem* **85**, 2243–2250. <https://doi.org/10.1002/cplu.202000373>.
25. Collie, G.W., Lombardo, C.M., Yoo, S.H., Pulka-Ziach, K., Gabelica, V., Mackereth, C.D., Rosu, F., and Guichard, G. (2021). Crystal structures capture multiple stoichiometric states of an aqueous self-assembling oligourea foldamer. *Chem. Commun. (Camb)* **57**, 9514–9517. <https://doi.org/10.1039/D1CC03604A>.
26. Douat-Casassus, C., Pulka, K., Claudon, P., and Guichard, G. (2012). Microwave-enhanced solid-phase synthesis of N,N'-linked aliphatic oligoureas and related hybrids. *Org. Lett.* **14**, 3130–3133. <https://doi.org/10.1021/ol3012106>.
27. Teysnières, E., Corre, J.P., Antunes, S., Rougeot, C., Dugave, C., Jouvion, G., Claudon, P., Mikaty, G., Douat, C., Goossens, P.L., and Guichard, G. (2016). Proteolytically stable foldamer mimics of host-defense peptides with protective activities in a murine model of bacterial infection. *J. Med. Chem.* **59**, 8221–8232. <https://doi.org/10.1021/acs.jmedchem.6b00144>.
28. Snook, C.F., Woolley, G.A., Oliva, G., Patabhi, V., Wood, S.F., Blundell, T.L., and Wallace, B.A. (1998). The structure and function of antimioeblin I, a proline-rich membrane-active polypeptide. *Structure* **6**, 783–792. [https://doi.org/10.1016/s0969-2126\(98\)00079-3](https://doi.org/10.1016/s0969-2126(98)00079-3).
29. Portella, G., and de Groot, B.L. (2009). Determinants of water permeability through nanoscopic hydrophilic channels. *Biophys. J.* **96**, 925–938. <https://doi.org/10.1016/j.bpj.2008.09.059>.
30. Mishra, V.K., Palgunachari, M.N., Krishna, R., Glushka, J., Segrest, J.P., and Anantharamaiah, G.M. (2008). Effect of leucine to phenylalanine substitution on the nonpolar face of a class A amphipathic helical peptide on its interaction with lipid: high resolution solution NMR studies of 4F-dimyristoylphosphatidylcholine discoidal complex. *J. Biol. Chem.* **283**, 34393–34402. <https://doi.org/10.1074/jbc.M806384200>.
31. Lombardo, C.M., Collie, G.W., Pulka-Ziach, K., Rosu, F., Gabelica, V., Mackereth, C.D., and Guichard, G. (2016). Anatomy of an oligourea six-helix bundle. *J. Am. Chem. Soc.* **138**, 10522–10530. <https://doi.org/10.1021/jacs.6b05063>.
32. Dutta, C., Chakraborty, K., and Sinha Roy, R. (2015). Engineered nanostructured facial lipopeptide as highly efficient molecular transporter. *ACS Appl. Mater. Interfaces* **7**, 18397–18405. <https://doi.org/10.1021/acsami.5b04392>.
33. Biswas, A., Chakraborty, K., Dutta, C., Mukherjee, S., Gayen, P., Jan, S., Mallick, A.M., Bhattacharya, D., and Sinha Roy, R. (2019). Engineered histidine-enriched facial lipopeptides for enhanced intracellular delivery of functional siRNA to triple negative breast cancer cells. *ACS Appl. Mater. Interfaces* **11**, 4719–4736. <https://doi.org/10.1021/acsami.8b13794>.
34. Chakraborty, K., Dutta, C., Mukherjee, S., Biswas, A., Gayen, P., George, G., Raghothama, S., Ghosh, S., Dey, S., Bhattacharya, D., et al. (2018). Engineering ionophore gramicidin-inspired self-assembled peptides for drug delivery and cancer nanotherapeutics. *Adv. Therap.* **1**, 1800018. <https://doi.org/10.1002/adtp.201800018>.
35. Shen, J., Ye, R., Romanies, A., Roy, A., Chen, F., Ren, C., Liu, Z., and Zeng, H. (2020). Aquafoldmer-based aquaporin-like synthetic water channel. *J. Am. Chem. Soc.* **142**, 10050–10058. <https://doi.org/10.1021/jacs.0c02013>.
36. Shen, Y.X., Song, W.C., Barden, D.R., Ren, T., Lang, C., Feroz, H., Henderson, C.B., Saboe, P.O., Tsai, D., Yan, H., et al. (2018). Achieving high permeability and enhanced selectivity for Angstrom-scale separations using artificial water channel membranes. *Nat. Commun.* **9**, 2294. <https://doi.org/10.1038/s41467-018-04604-y>.
37. Barboiu, M., Le Duc, Y., Gilles, A., Cazade, P.A., Michau, M., Marie Legrand, Y., Van Der Lee, A., Coasne, B., Parviz, P., Post, J., and Fyles, T. (2014). An artificial primitive mimic of the gramicidin-A channel. *Nat. Commun.* **5**, 4142. <https://doi.org/10.1038/ncomms5142>.
38. Rusinova, R., Kim, D.M., Nimigeon, C.M., and Andersen, O.S. (2014). Regulation of ion channel function by the host lipid bilayer examined by a stopped-flow spectrofluorometric assay. *Biophys. J.* **106**, 1070–1078. <https://doi.org/10.1016/j.bpj.2014.01.027>.
39. Posson, D.J., Rusinova, R., Andersen, O.S., and Nimigeon, C.M. (2018). Stopped-flow fluorometric ion flux assay for ligand-gated ion channel studies. *Methods Mol. Biol.* **1684**, 223–235. [https://doi.org/10.1007/978-1-4939-7362-0\\_17](https://doi.org/10.1007/978-1-4939-7362-0_17).
40. Lee, K.C.B., Siegel, J., Webb, S.E.D., Lévêque-Fort, S., Cole, M.J., Jones, R., Dowling, K., Lever, M.J., and French, P.M.W. (2001). Application of the stretched exponential function to fluorescence lifetime imaging. *Biophys. J.* **81**, 1265–1274. [https://doi.org/10.1016/S0006-3495\(01\)75784-0](https://doi.org/10.1016/S0006-3495(01)75784-0).
41. Leite, N.B., Aufderhorst-Roberts, A., Palma, M.S., Connell, S.D., Ruggiero Neto, J.R., and Beales, P.A. (2015). PE and PS lipids synergistically enhance membrane poration by a peptide with anticancer properties. *Biophys. J.* **109**, 936–947. <https://doi.org/10.1016/j.bpj.2015.07.033>.
42. Saha, T., Gautam, A., Mukherjee, A., Lahiri, M., and Talukdar, P. (2016). Chloride transport through supramolecular barrel-roseette ion channels: lipophilic control and apoptosis-inducing activity. *J. Am. Chem. Soc.* **138**, 16443–16451. <https://doi.org/10.1021/jacs.6b10379>.
43. Ren, C., Zeng, F., Shen, J., Chen, F., Roy, A., Zhou, S., Ren, H., and Zeng, H. (2018). Pore-forming mono-peptides as exceptionally active

- anion channels. *J. Am. Chem. Soc.* **140**, 8817–8826. <https://doi.org/10.1021/jacs.8b04657>.
44. Morgan, H., Lonsdale, J.T., and Alder, G. (1990). Polarity-dependent voltage-gated porin channels from *Escherichia coli* in lipid bilayer membranes. *Biochim. Biophys. Acta* **1021**, 175–181. [https://doi.org/10.1016/0005-2736\(90\)90031-i](https://doi.org/10.1016/0005-2736(90)90031-i).
45. Benndorf, K. (1989). A reinterpretation of Na channel gating and permeation in terms of a phase transition between a transmembrane S4  $\alpha$ -helix and a channel-helix. *Eur. Biophys. J.* **17**, 257–271. <https://doi.org/10.1007/BF00254283>.
46. Aldrich, R.W., and Stevens, C.F. (1987). Voltage-dependent gating of single sodium channels from mammalian neuroblastoma cells. *J. Neurosci.* **7**, 418–431. <https://doi.org/10.1523/JNEUROSCI.07-02-00418.1987>.
47. Mastrorarde, D.N. (2005). Automated electron microscope tomography using robust prediction of specimen movements. *J. Struct. Biol.* **152**, 36–51. <https://doi.org/10.1016/j.jsb.2005.07.007>.
48. Punjani, A., Rubinstein, J.L., Fleet, D.J., and Brubaker, M.A. (2017). cryoSPARC: algorithms for rapid unsupervised cryo-EM structure determination. *Nat. Methods* **14**, 290–296. <https://doi.org/10.1038/nmeth.4169>.
49. Zheng, S.Q., Palovcak, E., Armache, J.P., Verba, K.A., Cheng, Y., and Agard, D.A. (2017). MotionCor2: anisotropic correction of beam-induced motion for improved cryo-electron microscopy. *Nat. Methods* **14**, 331–332. <https://doi.org/10.1038/nmeth.4193>.
50. Rohou, A., and Grigorieff, N. (2015). CTFFIND4: fast and accurate defocus estimation from electron micrographs. *J. Struct. Biol.* **192**, 216–221. <https://doi.org/10.1016/j.jsb.2015.08.008>.
51. Schneider, S., Licsandru, E.D., Kocsis, I., Gilles, A., Dumitru, F., Moulin, E., Tan, J., Lehn, J.M., Giuseppone, N., and Barboiu, M. (2017). Columnar self-assemblies of triarylmines as scaffolds for artificial biomimetic channels for ion and for water transport. *J. Am. Chem. Soc.* **139**, 3721–3727. <https://doi.org/10.1021/jacs.6b12094>.